We are IntechOpen,
the world's leading publisher of
Open Access books
Built by scientists, for scientists

4,800
Open access books available

122,000
International authors and editors

135M
Downloads

Our authors are among the

154
Countries delivered to

TOP 1%
most cited scientists

12.2%
Contributors from top 500 universities

CLARIVATE ANALYTICS
BOOK CITATION INDEX
INDEXED

WEB OF SCIENCE™

Selection of our books indexed in the Book Citation Index
in Web of Science™ Core Collection (BKCI)

Interested in publishing with us?
Contact book.department@intechopen.com

Countermeasure for High Level Sound Generated from Boiler Tube Bank Duct

Masaaki Mori and Kunihiko Ishihara

Abstract

Heat exchangers and boilers are widely used in various plants such as power plants and chemical plants. In the heat exchanger and the boiler, a high level sound is sometimes generated from the tube bank installed in a duct. In tube banks, warm gas flows outside of the tube, and due to the external flow around tube banks, the Karman vortex shedding occurs. At a certain frequency of the Karman vortex shedding that depends on the flow velocity, the resonance phenomenon called the self-sustained tone occurs. The self-sustained tone might cause noise problems in the surroundings, losses due to plant shutdown, etc. For suppression of the self-sustained tone, insertion of baffle plates in the tube bank is generally used. Although the insertion of baffle plates has been adopted for a long time, it is difficult to decide the effective insertion positions. On the other hand, a method using perforated plates has been proposed for the suppression of the self-sustained tones. In this chapter, we review the generation mechanism of the self-sustained tone clarified experimentally and numerically, and the methods for suppressing a self-sustained tone using baffle plates and perforated plates.

Keywords: self-sustained tone, high level sound, acoustic resonance, lock-in phenomenon, countermeasure, baffle plate, perforated plate

1. Introduction

Heat exchangers and boilers are widely used in various plants such as power plants and chemical plants. In heat exchangers such as boilers and gas heaters, a high level sound is sometimes generated and it results in a serious problem such as a plant shutdown or non-operation. A high level sound is generated in tube banks installed in a duct. In tube banks, water flows inside of tubes, warm gas flows outside of tubes, and Karman vortex shedding occurs. The vortex shedding frequency depends on the flow velocity. In contrast, a resonance frequency called an acoustic natural frequency, which is independent of the flow velocity, is determined by the duct size and the sound speed. When the two frequencies coincide, a resonance phenomenon occurs at a certain velocity [1–9]. Ziada and Oengören [10] have shown that vortex excitation results from the formation of periodic vortices in the space between tubes by visualization experiments in the waterway. Hamakawa et al. [11] focused on effect of arrangement of tube banks, and investigated the characteristics of vortex shedding and acoustic resonance from in-line and staggered tube banks.

When a resonance phenomenon occurs at a certain velocity, if the acoustic damping is small, a high level sound continues as flow velocity increases. This phenomenon is called the self-sustained tone [12, 13]. The self-sustained tone might cause the surrounding noise problem, and also cause plant shutdown and, hence, production losses, etc.

For a countermeasure of the self-sustained tone, a method of inserting a partition plate called a baffle plate inside the duct is generally used. In this method, the baffle plate inserted inside the duct is assumed to increase the natural frequency of the duct, detune the frequency of the vortex shedding from the tube bank and the acoustic natural frequency of the duct, and suppress the resonance phenomenon [14–16]. However, Ishihara et al. [12] demonstrated that the natural frequency of the duct decreases by inserting the baffle plate, and a decision of an appropriate insertion position of the baffle plate is not easy. Hamakawa et al. [16] have investigated the effect of the baffle plate on the acoustic resonance generation from in-line tube banks with small cavity, and they clarified that although sound pressure level of an acoustic mode perpendicular to the flow (lift mode) is suppressed by a baffle plate, that of an acoustic mode parallel to the flow (drag mode) increases. Ishihara and Takahashi proposed that flexible walls such as rubber boards are set on the duct walls for suppressing the self-sustained tone [17]. They expected that the vibration of the flexible walls damp the lift resonance mode when self-sustained tone is generated. They demonstrated that the suppression effect of the rubber sheet appeared when the tension of it is small and it is located at just the tube bank and downstream of the tube bank. On the other hand, to suppress the self-sustained tones, a method using perforated plates and cavities has been proposed by Ishihara and Nakaoka [13]. A perforated plate has long been used in various noise-control applications, such as vehicle exhaust systems, ducts, hearing protection devices, and acoustic panels, because it is well known that perforated plates have an acoustic damping effect [18–20]. Ishihara and Nakaoka [13] thought that a resonance mode perpendicular to the flow (lift mode) might be suppressed by a damping effect of perforated plates, when the self-sustained tone occurred.

In this chapter, we review the generation mechanism of the self-sustained tone clarified experimentally and numerically, and the methods for suppressing a self-sustained tone using baffle plates and perforated plates.

2. Generation mechanism of self-sustained tone

2.1 Self-sustained tone

The Karman vortex shedding frequency fv is generally proportional to the flow velocity and the natural frequency of the duct fa is constant value determined by the duct size and the sound speed. When the flow velocity increases, the fv approaches fa. Before the fv reaches the fa, the vortex shedding frequency suddenly locks on to the natural frequency of the duct. The resultant high level sound occurs at or nearly at the natural frequency of the duct, and this phenomenon is called a lock-in or lock-on. There are many studies on the excitation mechanism of a lock-in or lock-on phenomenon in the tube bank [1–11, 21, 22].

The relation between frequency and flow velocity in a lock-in phenomenon is represented in **Figure 1**. A high level sound called a self-sustained tone occurs due to a lock-in phenomenon [12, 13]. In a lock-in phenomenon, as shown in **Figure 1**, the frequency slightly rises as the flow velocity increases. Furthermore, the lock-in occurs at a certain flow velocity, and does not occur in accordance with the large acoustic damping of the duct if the flow velocity increases. However, with the small
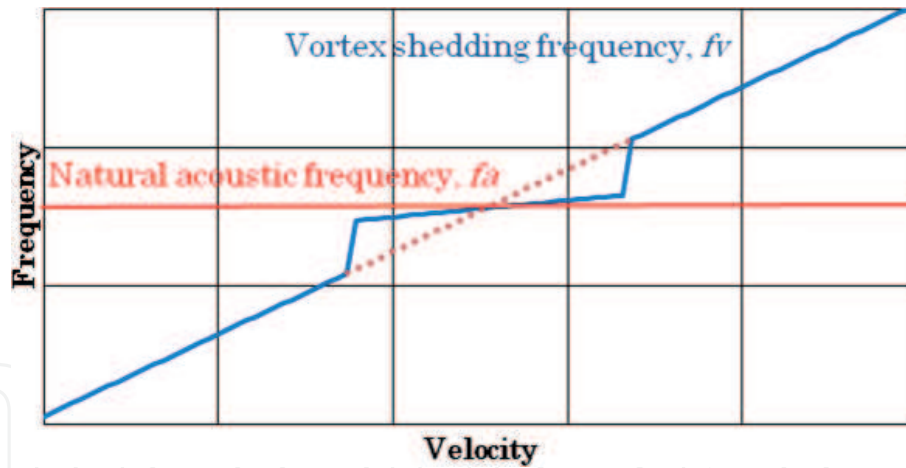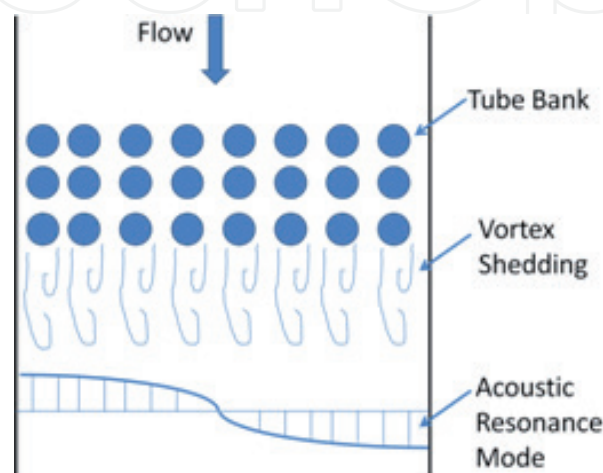
Figure 1.
Relation between frequency and velocity in the case of lock-in phenomenon.

acoustic damping of the duct, the lock-in continues as the flow velocity increases, and the sound pressure level remains high [13]. **Figure 2** shows that when the shedding frequency of the strong vortices generated in the tube bank almost coincides with the acoustic resonance frequency of the duct, the strong sound field in the duct is excited. As a result, the vortices and the sound field in the duct cause the strong interaction. This phenomenon is a self-excited mechanism.

Also, focused on the self-excited acoustic resonance of two side-by-side cylinders in a duct, the mechanism of the self-excited acoustic resonance is investigated by experiments and numerical solutions [21, 22]. It was found that dynamic lift fluctuation on the cylinders and strong in-phase vortex shedding synchronization are generated by the acoustic resonance. Shahab Khushnood et al. reviewed and summarized the flow-induced vibrations and acoustic resonance in heat exchanger tube bundles [23].

2.2 Setup of experiment

Ishihara et al. [12, 13] performed the experiments to investigate the self-sustained tone. **Figure 3(a)** and **(b)** represents the setup of the experiment and the tube bank. The duct is made of acrylic plates that have a thickness of 1 cm. The tube bank consists of an array of bronze tubes whose diameter is D = 6 mm. The array geometry is represented in **Figure 3(b)**, where the spacings T/D and L/D are

Figure 2.
*Acoustic resonance and lock-in phenomenon.*
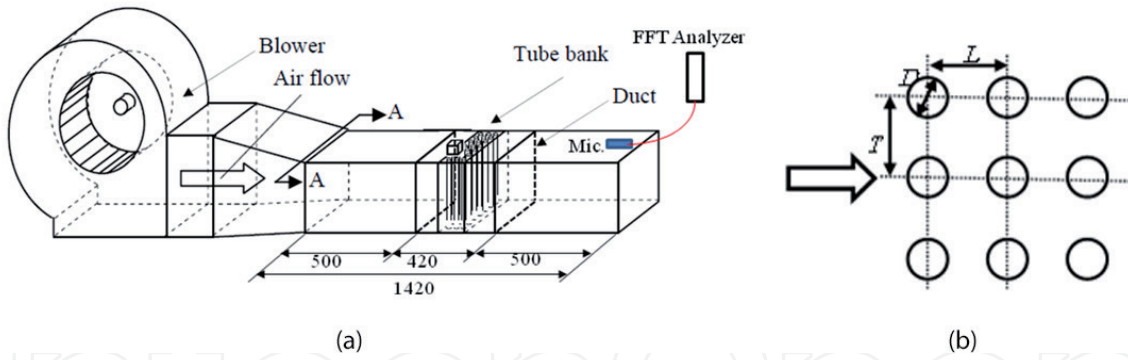
Figure 3.
Setup of experiment and array geometry of tube bank [24]. (a) Setup of experiment. (b) Array geometry of tube bank.

2.0. In the tube bank, there are 9 rows of tubes in the flow direction and 19 tubes in the width direction, which is perpendicular to the flow, and the length in the flow direction is 102 mm. The sound pressure signal is measured using the microphone set near the duct outlet as shown in **Figure 3(a)**, and converted to frequency domain with FFT analyzer. The flow velocity is changed by controlling the rotational speed of the blower using the inverter. A high level sound is generated when the shedding frequency of vortices generated in the tube bank nearly coincides with the acoustic natural frequency of the duct system. A flow velocity measurement hole was provided at a position 125 mm upstream of the tube group, and the flow velocity (U) was also measured by using a hot wire anemometer. The gap flow velocity V_g is obtained from the continuous equation, defined by the flow velocity U and the ratio of the area of the duct outlet to the area of the tube bank clearance which is 234 mm (Duct width)/(234 mm – 19 (number of tubes in the width direction)*6 mm (tube diameter)) = 1.95, and represented by V_g = 1.95 U. The measurement frequency ranges from 100 to 2000 Hz. The sound pressures signal is measured with the sampling frequency of 10,000 Hz, the number of averages of 1000, and the frequency resolution of 20 Hz.

2.3 Results of experiments

The sound pressure spectrum at each gap velocity (11.4, 15.7, 19.6, and 21.3 m/s) is shown in **Figure 4**. As shown in **Figure 4**, the self-sustained tone is slightly generated at V_g = 19.6 m/s, and is clearly generated at V_g = 21.3 m/s. The peak frequency of the self-sustained tone is 740 Hz. The relation between overall sound pressure level and the gap velocity obtained from the experiments is represented in **Figure 5**. Sound pressure level generated by a flow in a duct generally follows the 5–8th power laws [13], and the sound pressure level generated in the duct in this experiment follows the 5th power law. Sound following the 5th power law is the ordinary aerodynamic sound. The sound pressure level rises as the gap velocity increases by following the 5th power law when the self-sustained tone is not generated (when the gap velocity is lower than 20 m/s). However, the sound pressure level is over 100 dB when the self-sustained tone is generated (when the gap velocity is higher than 20 m/s). **Figure 5** represents that when the gap flow velocity is over 22 m/s, the overall sound pressure level remains high and is over 110 dB [15]. The self-excited tone is generated at the gap velocity over 20 m/s, and it indicated that if the Strouhal number St is assumed to be 0.22, the vortex shedding frequency f_v is f_v = $St * V_g/D$ = 0.22 * $20/0.006$ = 733 Hz. Meanwhile, the resonance frequency f_a in the width direction of the duct is $f_a = C/2L$ = 340/2/0.234 = 726.5 Hz.
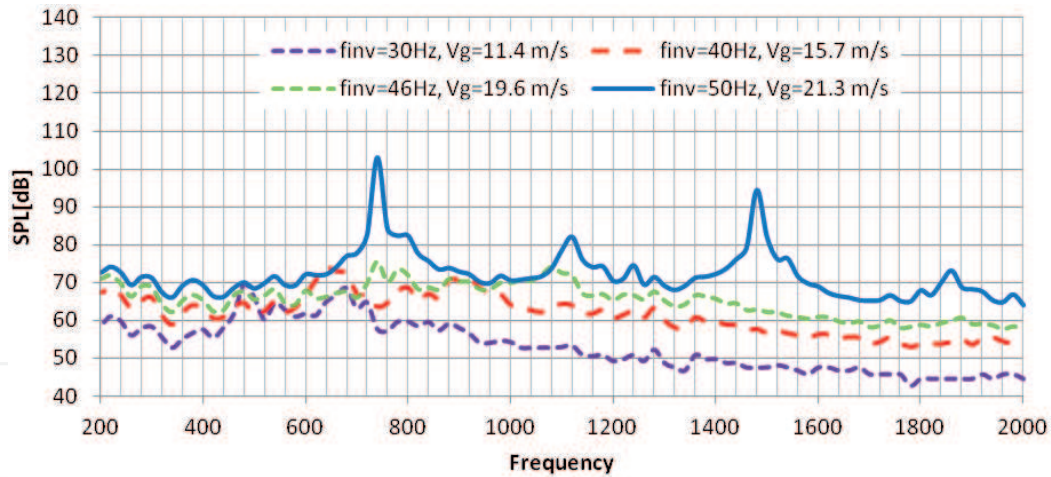
Figure 4.
Spectra of sound pressure level.
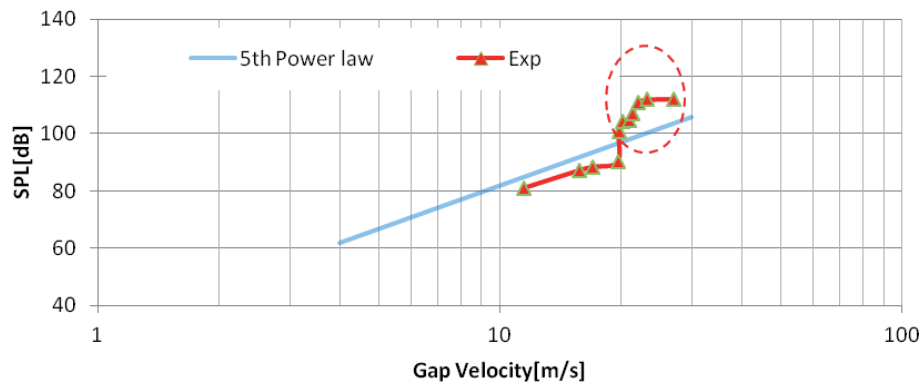
Figure 5.
Relation between overall sound pressure level (200–2000 Hz) and the gap velocity.

Taking the combined mode in the longitudinal direction into consideration, the resonance frequency f_a is obtained from Eq. (1) and equals 736.3 Hz, which is very close to the frequency of excitation at 740 Hz obtained from the experiments.

$$f_a = \frac{c}{2}\sqrt{\left(\frac{1}{l_x}\right)^2 + \left(\frac{m}{l_y}\right)^2} = \frac{340}{2}\sqrt{\left(\frac{1}{0.234}\right)^2 + \left(\frac{1}{1.42}\right)^2} = 736.3 \text{ Hz} \qquad (1)$$

Here, l_x and l_y denote the longitudinal duct length and the duct width, respectively.

2.4 Unsteady CFD simulations

Mori et al. [24] performed compressible CFD simulations to capture the self-sustained tone and compare the simulation results with the measurements [13]. They confirmed that the self-sustained tone at the acoustic mode in the width direction of the duct occurs, and the sound pressure level does not follow the 5th power law when the gap velocity is high, as in the experiments. Unsteady flow fields in the duct are simulated in the paper. Inflow velocities are U = 5.846, 7.026, 8.051, 8.564, 9.590, 10.923, and 13.846 m/s, and correspond to the gap velocities, V_g = 11.4, 13.7, 15.7, 16.7, 18.7, 21.3, and 27.0 m/s, respectively. **Figure 6** represents the CFD model that is a three-dimensional computational domain. Reynolds number Re_D is based on the gap velocity V_g, and ranges from 4600 to 10,800.

5
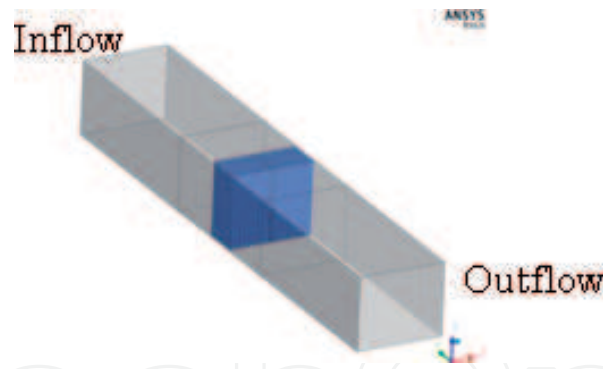
Figure 6.
CFD model [24].

Unsteady flow fields are calculated using the commercial CFD code ANSYS Fluent version 17.0. An implicit pressure-based coupled solver with second-order numerical accuracy in both space and time and compressible LES (Dynamic Smagorinsky model) calculation features have been applied. The interaction between the flow and acoustic fields need to be solved when the resonance or self-sustained tone is generated, a high level sound is generated, and the monitor point is near the noise source region. Therefore, the acoustic pressure is directly extracted from the unsteady compressible CFD simulations [25].

The origin of the Cartesian coordinate is placed at the center of the inflow boundary. The cell spacing adjacent to the wall is 0.00025 m. In the wake region near the tube bank, the cell spacing is about 0.002 m. In the far wake region, the cell spacing is stretched to 0.006 m. The domain contains 4,944,100 cells and 5,156,304 nodes. CFD simulation conditions are shown in **Table 1**.

Steady-state simulations were performed using Spalart-Allmaras (S-A) turbulence model and then used as initial conditions of transient LES simulations. The time step size corresponds to the non-dimensional time step based on f_v, 0.00733. To convert the acoustic pressure time histories obtained from CFD simulations into the frequency spectra, the discrete Fourier transform (DFT) has been applied. The acoustic pressure is extracted from 2500 steps (from t = 0.05 to 0.1 s). The sampling period is 2e-5 s.

Instantaneous snapshots of vorticity fields at $Z = 0$ plane are shown in **Figure 7(a)** and **(b)**, for the cases of V_g = 11.4 m/s and V_g = 21.3 m/s. A vortex street is formed downstream by vortices shed in the tube bank. At V_g = 21.3 m/s, the strength of the vortices is larger than at V_g = 11.4 m/s. Instantaneous snapshots of static pressure fields are represented in **Figure 8**. **Figure 8** shows that the value of the static pressure on the upstream side of the tube bank is larger than that on the downstream side, and distinguishing the sound pressure from the static pressure seems to be difficult. Thus, the fluctuation pressure is defined as follows to distinguish easily between the sound pressure and the static pressure [24].

$$dp = p_s - p_{mean} \tag{2}$$

|	
Inflow boundary conditions	Steady velocity [m/s]: 11.4, 13.7, 15.7, 16.7, 18.7, 21.3 and 27.0
	Temperature [K]:300
Outflow boundary conditions	Zero pressure and Non-reflective boundary condition
Wall conditions	No-slip and Adiabatic
Time step size [sec]	1e-5
Calculation Steps	10000

Table 1.
CFD simulation conditions.
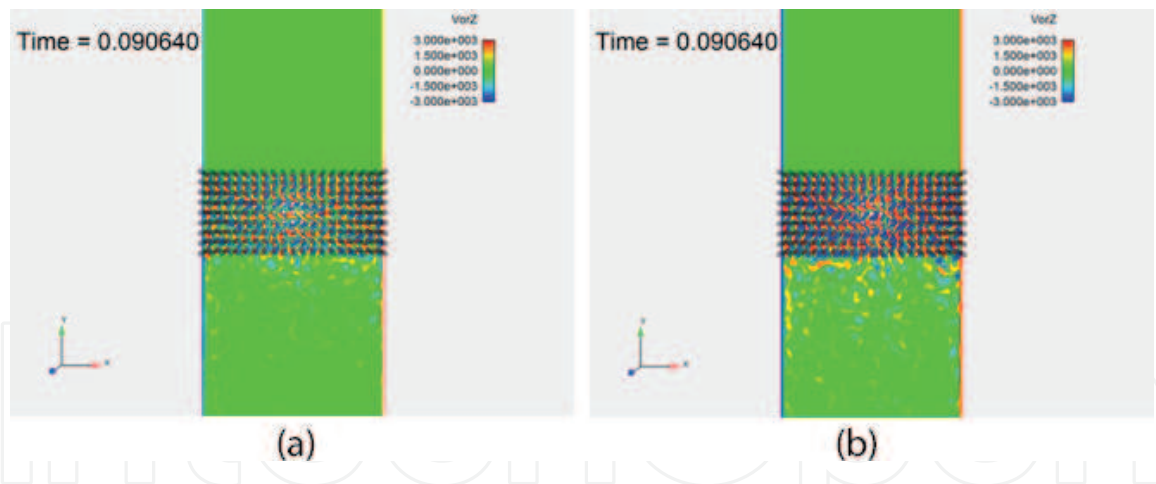
Figure 7.
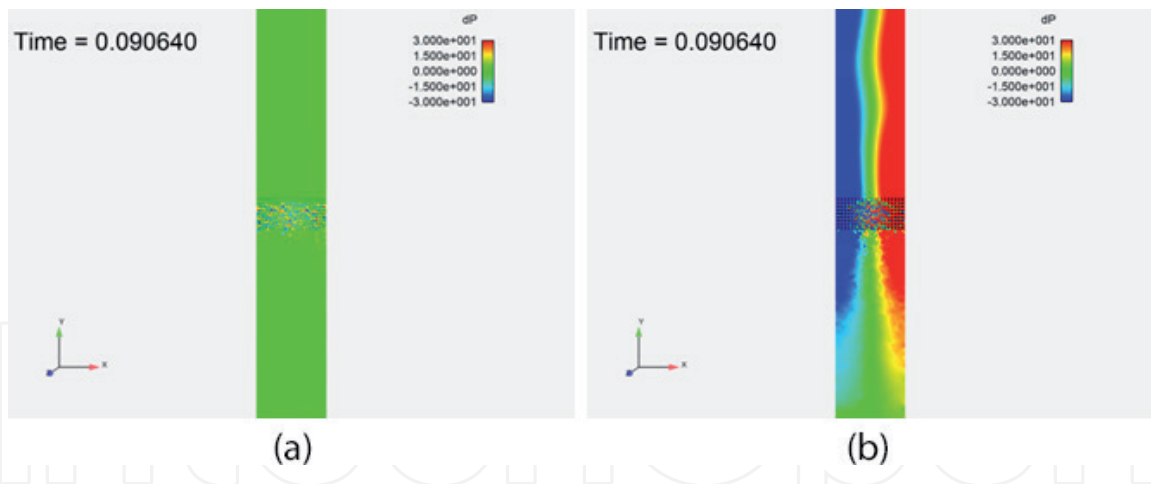*Vorticity fields. (a) V_g = 11.4 m/s. (b) V_g = 21.3 m/s.*

Here, p_s denotes the static pressure which is defined by $p_s = p - p_0$, p_{mean} denotes the time-averaged pressure, and p_0 denotes the ambient pressure. Instantaneous snapshots of fluctuation pressure field at Z = 0 plane obtained from the unsteady CFD simulations are represented in **Figure 9**. The value of the fluctuation pressure at V_g = 21.3 m/s is much larger than at V_g = 11.4 m/s. At V_g = 21.3 m/s, the pressure fluctuation clearly represents the resonance mode in the duct width direction.

The frequency spectra of SPL are monitored on the wall of the duct near the outflow boundary, and represented in **Figure 10**. The self-sustained tone is generated when the gap velocity V_g is 21.3 m/s, and the self-sustained tone is not generated when the gap velocity V_g is 11.4 m/s. The peak frequency of the self-sustained tone is about 740 Hz and its high harmonic frequency, 1480 Hz, when the gap velocity V_g is 21.3 m/s. This frequency, 740 Hz, is close to the resonance frequency in the duct width direction, 726.5 Hz, and that in the combined mode in the longitudinal direction, 736.3 Hz, as mentioned in Section 2.3. The resonance frequencies obtained from the theory (without the flow) and the CFD simulations or the experiments are slightly different because of the absence or presence of the flow. **Figure 1** shows that the slight increase of the resonance frequency occurs with an increase of the gap flow velocity [24]. The predicted SPL of the dominant tone at 740 Hz reasonably agrees with the measured one. The generation of the higher harmonic at 1480 Hz, which is surrounded by the red circle in **Figure 10**, is also predicted as in the experiments. The predicted SPL of the dominant tone, which is assumed to contribute most to the overall SPL when the self-sustained tone is generated, reasonably agrees with the measured one.
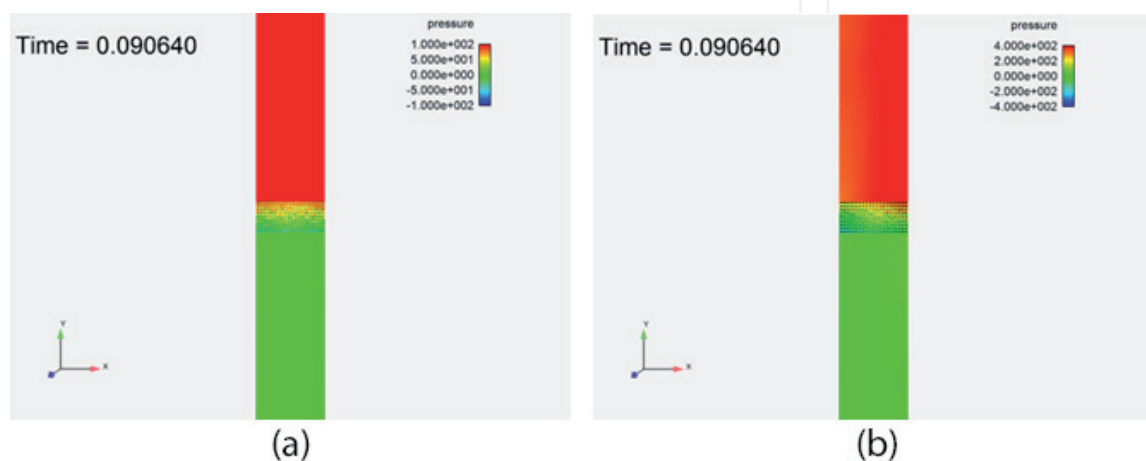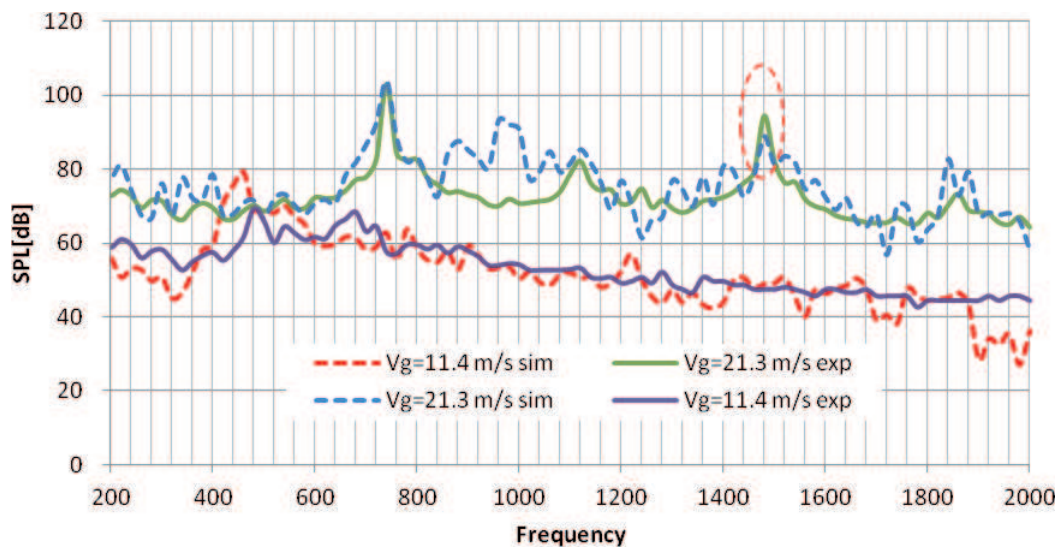

Figure 8.
*Static pressure fields. (a) V_g = 11.4 m/s. (b) V_g = 21.3 m/s.*

Figure 9.
*Fluctuation pressure fields. (a) V_g = 11.4 m/s. (b) V_g = 21.3 m/s.*

Figure 10.
Spectra of sound pressure level.

The relation between overall sound pressure level and the gap velocity obtained by both the simulations and experiments is represented in **Figure 11**. In both the simulations and experiments, when the gap velocity is low and below 20 m/s, the sound pressure level rises as the gap velocity increases by following the 5th power law. However,
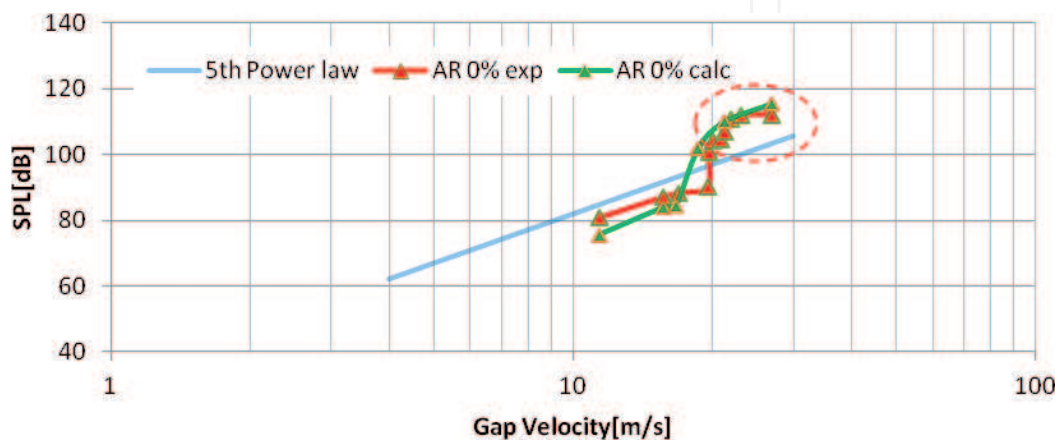
Figure 11.
Relation between overall sound pressure level (200–2000 Hz) and gap velocity.
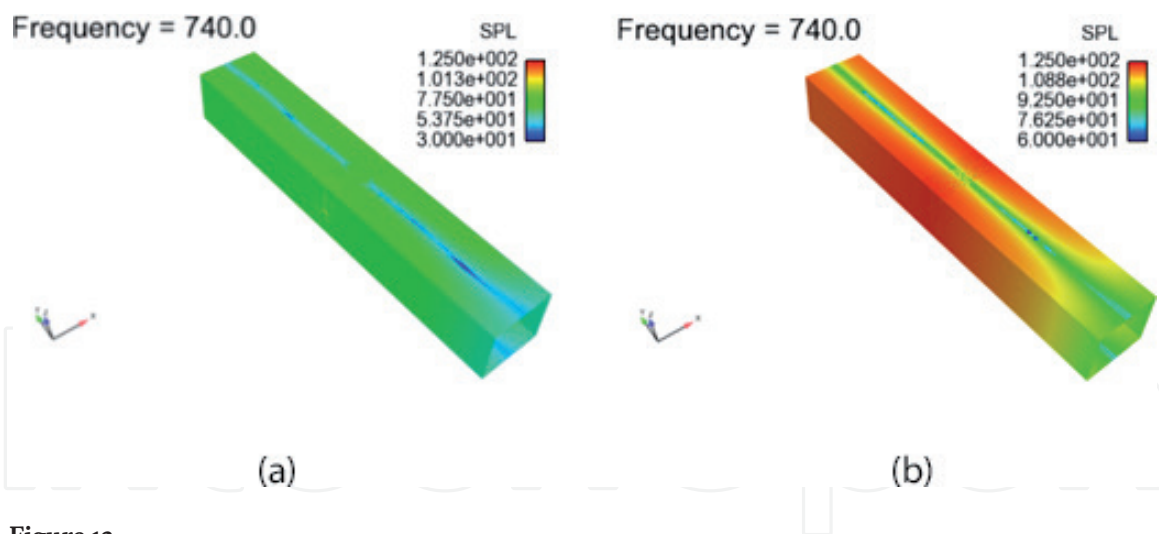
Figure 12.
*SPL on the wall of the duct ([24]). (a) V_g = 11.4 m/s. (b) V_g = 21.3 m/s.*

when the gap velocity is higher than 20 m/s, the self-sustained tone is generated and the sound pressure level is high and over 100 dB not by following the 5th power law. **Figures 10** and **11** represent that the sound pressure levels obtained by the simulations reasonably agree with those obtained by the experiments. **Figure 12** shows the SPLs on the wall of the duct at 740 Hz; these are extracted from the unsteady CFD simulations using DFT. As in the experiments, **Figure 12(b)** shows that when V_g = 21.3 m/s (the gap velocity is higher than 20 m/s), the SPL on the duct wall clearly represents the acoustic resonance mode in the duct width direction or the combined mode in the duct width and longitudinal directions. However, when V_g = 11.4 m/s (the gap velocity is lower than 20 m/s), the acoustic resonance mode is not clearly represented as shown in **Figure 12(a)**. The fluctuation pressure field shown in **Figure 9(b)** is consistent with the acoustic mode at 740 Hz shown in **Figure 12(b)**, which means that the dominant mode in the self-sustained tone is the acoustic mode in the duct width direction or the combined mode in the duct width and longitudinal directions, and is close to the acoustic mode obtained from the Eq. (1) and the experiments.

As shown in **Figures 10** and **11**, the simulations show a reasonable agreement with the experiments in terms of the generation prediction of the self-sustained tone.

3. Countermeasure for self-sustained tone using baffle plate

3.1 Setup of experiment

In this section, we describe the experiments performed by Ishihara et al. [12, 26]. They have investigated the appropriate insertion position of the baffle plate for the suppression of the self-sustained tone and the mechanism of suppressing the self-sustained tone by inserting the baffle plate. The setup of the experiment is shown in **Figure 3(a)** and the duct used in this experiment is shown in **Figure 13**. The tube bank consists of an array of bronze tubes whose diameter is D = 6 mm. The array geometry is represented in **Figure 3(b)**, where the spacings T/D and L/D are 2.0. In the tube bank, there are 5 rows of tubes in the flow direction and 18 tubes in the width direction, which is perpendicular to the flow, and the length in the flow direction is 60 mm. The sound pressure signal is measured using the microphone set near the duct outlet as shown in **Figure 3(a)**, and converted to frequency domain with FFT analyzer. One tube bank is installed in the duct in the present experiment as shown in **Figure 13**. The baffle plate with a length of 60 mm, thickness of 3 mm, and height of 200 mm is inserted in the center of the tube bank
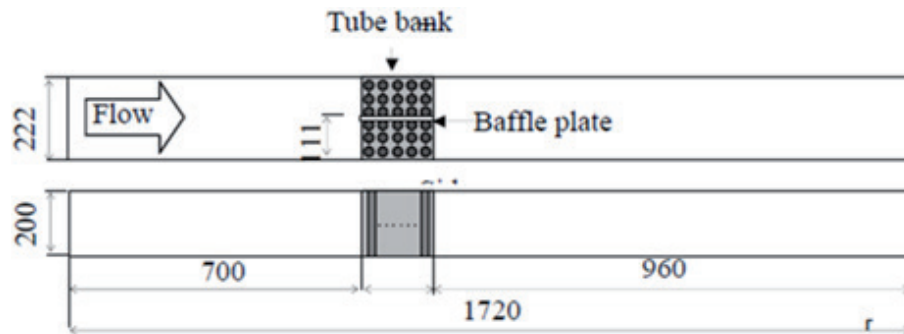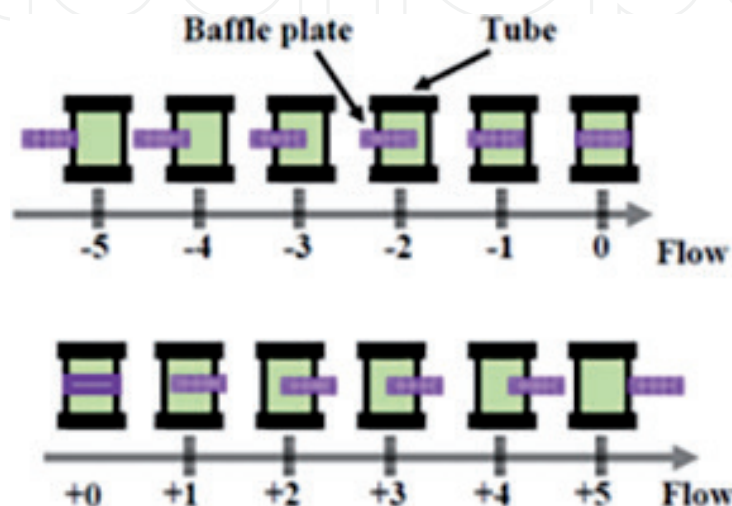
Figure 13.
Setup of experiment ([12]).

as shown in **Figure 13**. The position of this baffle plate is varied in the flow direction in increments of a row pitch (12 mm) in the tube array. The patterns of the baffle plate position are shown in **Figure 14**. An effective position of the baffle plate for suppressing the self-sustained tone is derived from this experiment.

3.2 Results of experiments

3.2.1 Natural frequency and peak frequency of self-sustained tone

Figure 15 represents the natural frequency of the duct and the peak frequency of the self-sustained tone. The vertical axis shows the frequency while the horizontal axis shows the pattern of the baffle plate positions as shown in this figure. The natural frequency of the duct can be obtained by the speaker test that was performed using the setup of the experiment shown in **Figure 13**. The peak frequency of the self-sustained tone was obtained by the ventilation experiment. The symbol △ shows the peak frequency in the case "with baffle plate". In this case, the self-sustained tone was not generated when the baffle plate positions are −1, 0, and + 1. Therefore, we cannot see the symbol △ in these positions. The natural frequency of the duct corresponds to the peak frequency of the self-sustained tone as represented in **Figure 15**. For a countermeasure of a self-sustained tone, a method involving the insertion of a baffle plate in the duct is generally adopted to suppress the self-sustained tone. This method is based on the idea that the baffle plate can prevent the resonance within the range of the usage flow velocity by introducing a new partition, thus increasing the natural frequency

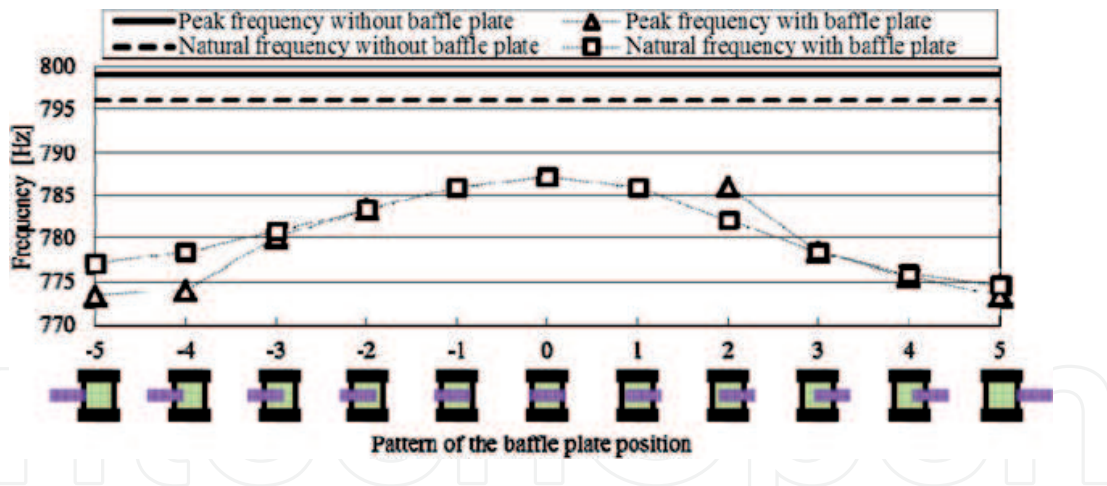**Figure 14.**
Pattern of baffle plate positions ([12]).

Figure 15.
Natural frequency and peak frequency ([12]).

of the duct [14, 15]. However, **Figure 15** represents that the natural frequency of the duct decreases by the insertion of the baffle plate regardless of the position in **Figure 15**, because the baffle plate cannot divide into two parts of the acoustic field of the duct due to a small length. If the baffle plate length is the same with the length of the duct, then the natural frequency becomes higher and doubles.

3.2.2 Onset gap velocity of self-sustained tone

Figure 16 represents the onset gap velocity of the self-sustained tone. The vertical axis shows the gap velocity of the tube bank when the self-sustained tone is generated and the horizontal axis shows the pattern of the baffle plate positions as shown in this figure. In patterns (−1, 0, and + 1) where the baffle plate is inserted in the entire tube bank, the self-sustained tone was not generated within the range of the flow velocity that the setup of experiment can produce. The self-sustained tone is not generated because vortices are assumed to become very small in patterns (−1, 0, +1) as described later. Furthermore, the onset gap velocity of the self-sustained tone shows a significantly different tendency between the upstream and the downstream positions of the baffle plate.
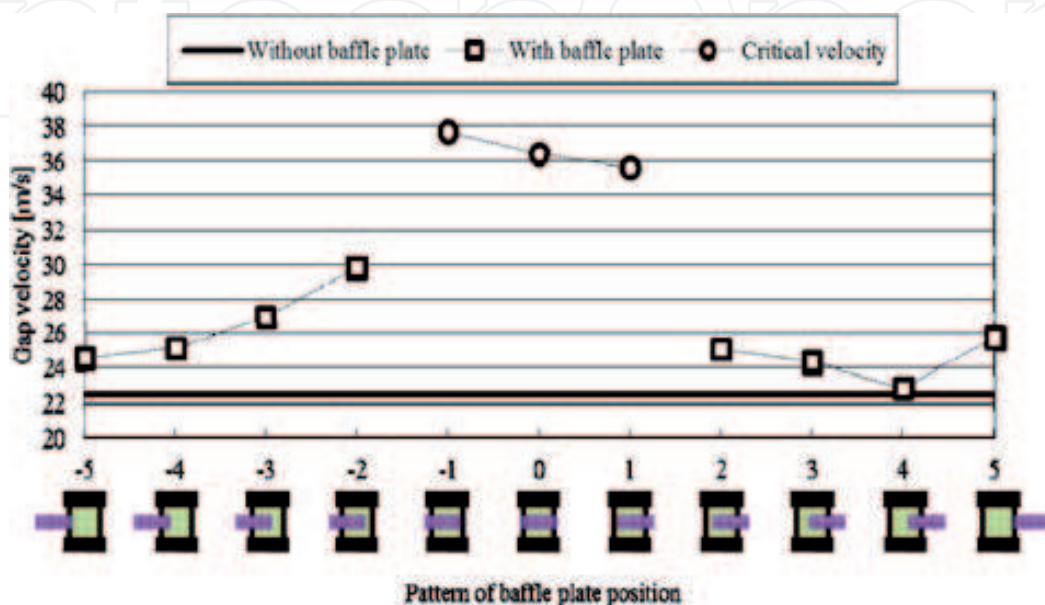

Figure 16.
*Gap velocity and pattern of baffle plate positions ([12]).*

The measurement position of the fluctuation velocity in the tube bank by the hot wire anemometer is shown in **Figure 17**. Because the baffle plate is inserted at the center of the tube bank, the hot wire probe is inserted in the neighboring flow channel. Additionally, the fluctuation velocity is measured between each tube row (12 mm interval). Measurement examples (the measurement position is 36 mm) of the fluctuation velocity U_f of the flow in the tube bank and SPL are shown in **Figures 18** and **19**. The vertical axis shows the fluctuation velocity of the flow and the horizontal axis shows the frequency. Two peaks (one sharp and the other dull) are represented in **Figures 18** and **19**. The sharp peak is due to the self-sustained tone and the dull peak is due to Karman vortex shedding as represented in **Figure 18**. The Karman vortex occurs in the tube bank, and the Strouhal number is about 0.13–0.19. The peak frequency of Karman vortex shedding is in proportion to the flow velocity and increases as the flow velocity increases. On the other hand, the peak frequency of the self-sustained tone coincides with the natural frequency of the duct, the sharp peak is assumed to correspond to the flow fluctuations related to the generation of the self-sustained tone. To distinguish the sharp peak from other peaks, it is referred to as "Excitation flow fluctuation" in this chapter. However, Karman vortices are generated and the excitation flow fluctuation is not generated if the baffle plate inserted in the entire tube bank suppresses the self-sustained tone.

*3.2.3 Suppression mechanism of self-sustained tone by baffle plate*

The sound power which the vortices add to the acoustic field of the duct is given by Eq. (3) from Howe [27]. The parameters are W: sound power [W], ρ: gas density [kg/m^3], $\vec{\omega}$: vorticity [rad/s], $\vec{U}$: flow velocity, [m/s], and $\vec{\varphi}$: particle velocity [m/s].

$$w = \rho \int (\vec{\omega} \times \vec{U}) \cdot \vec{\varphi} dV \qquad (3)$$

The particle velocity in the duct is given by the gradient of the sound pressure. Moreover, the phase of the particle velocity to the sound pressure progresses by 90 degrees. The particle velocity is therefore the maximum at the node of the acoustic pressure. In addition, the particle velocity is the largest in the center of the duct width. Karman vortices are strong in the tube bank, and that means the vorticity is large in the tube bank. In addition, the vorticity strongly depends on the fluctuation velocity U_f of the flow in the tube bank. Each parameter is controlled by inserting the baffle plate in the center of the duct where these two parameters (the particle velocity and vorticity) are large. As shown **Figure 12(b)**, the sound pressure level is the maximum on the duct wall and the sound pressure level is the minimum in
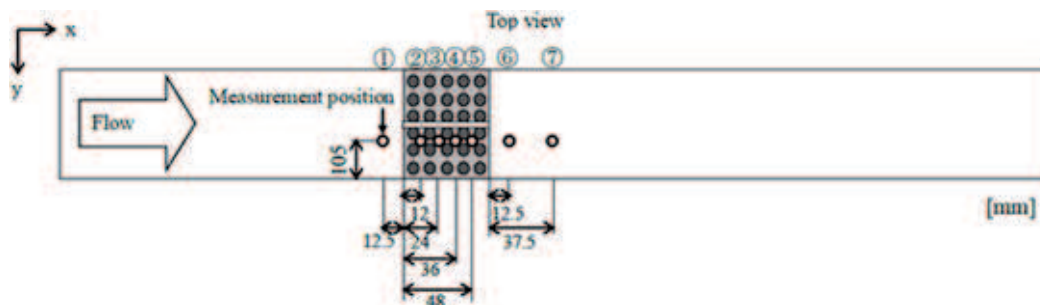
Figure 17.
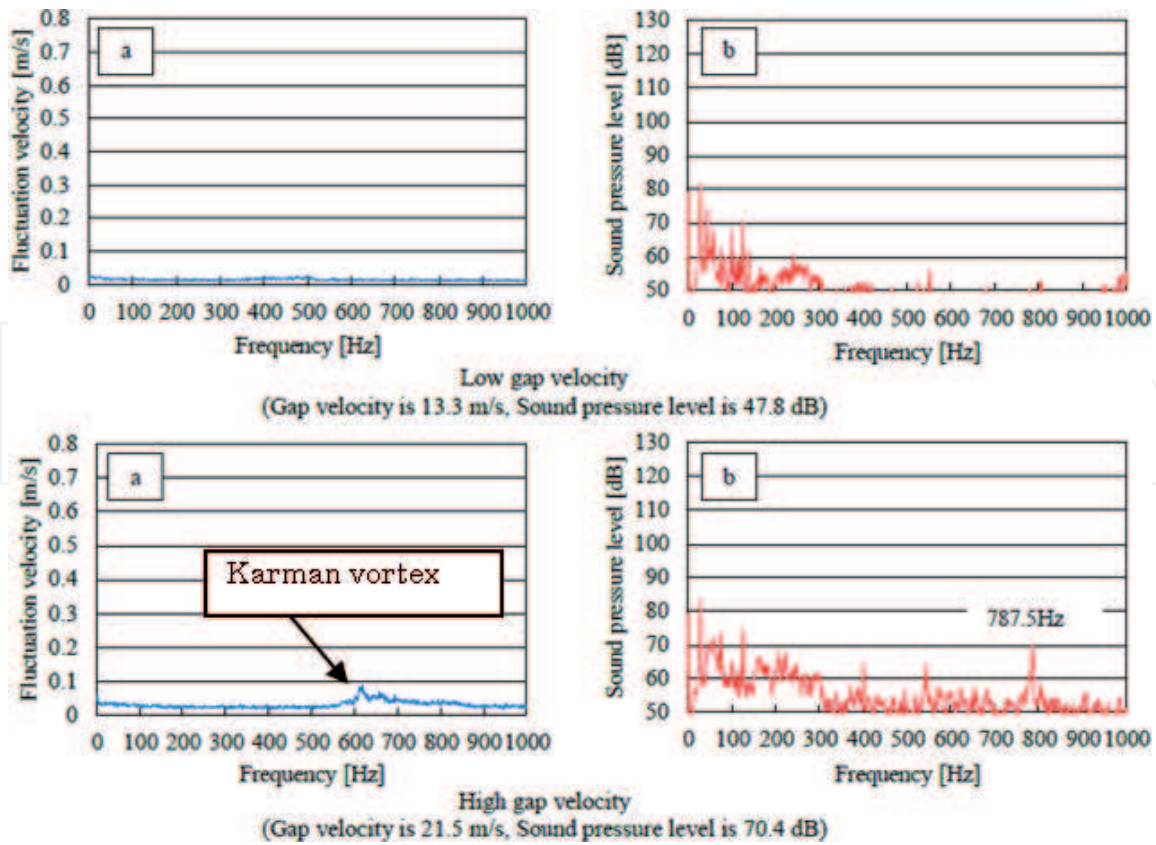*Measurement positions of fluctuation velocity in duct ([12]).*
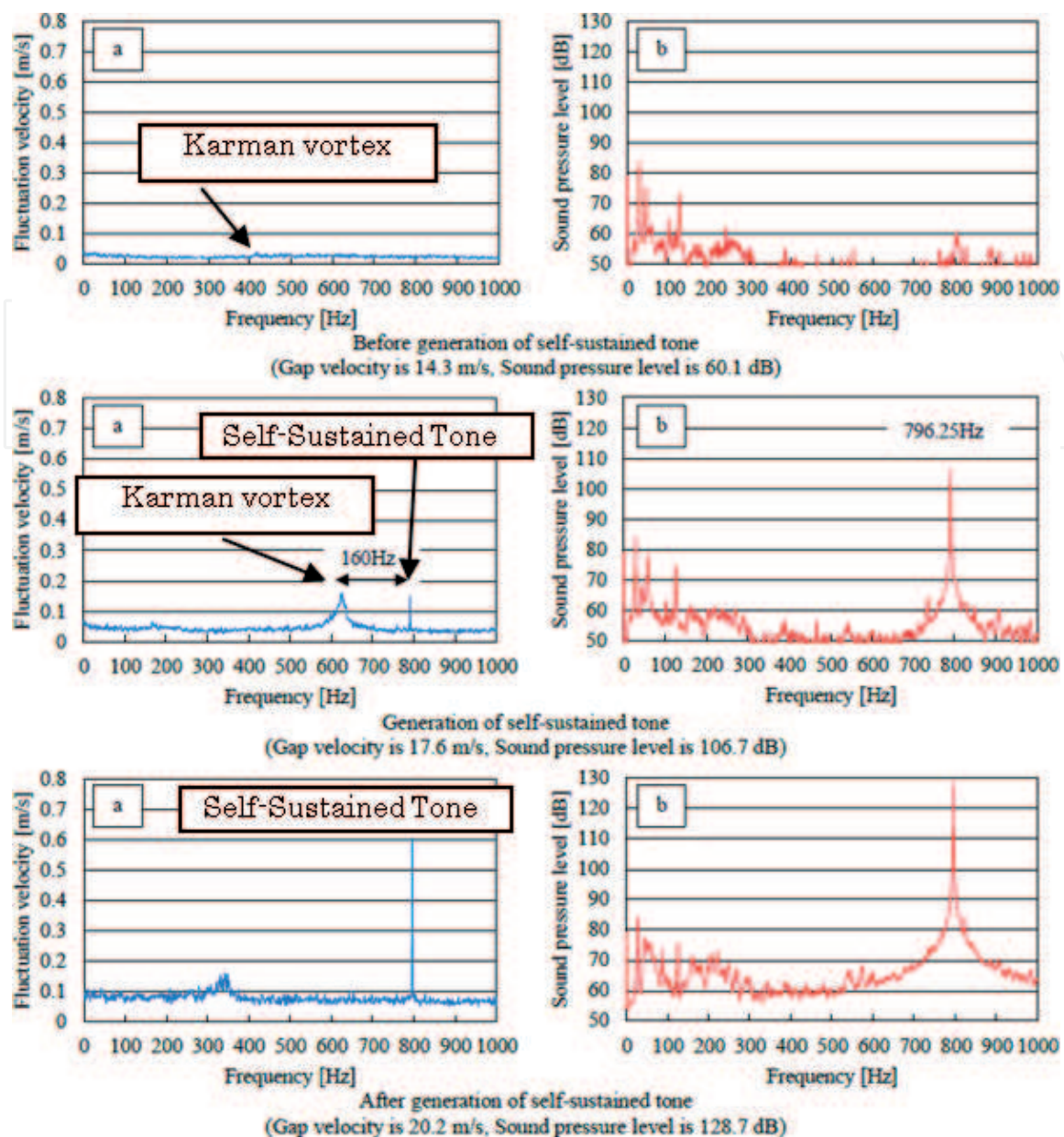
Figure 18.
The fluctuation velocity of flow and the sound pressure level at observation point ③ without the baffle plate ([26]).

the center of the duct, which means that the gradient of the sound pressure or the particle velocity is the maximum in the center of the duct and tube bank. Therefore, the vorticity and particle velocity decrease due to the baffle plate inserted in the duct; as a result, the sound power decreases. This is the suppression mechanism of the self-sustained tone.
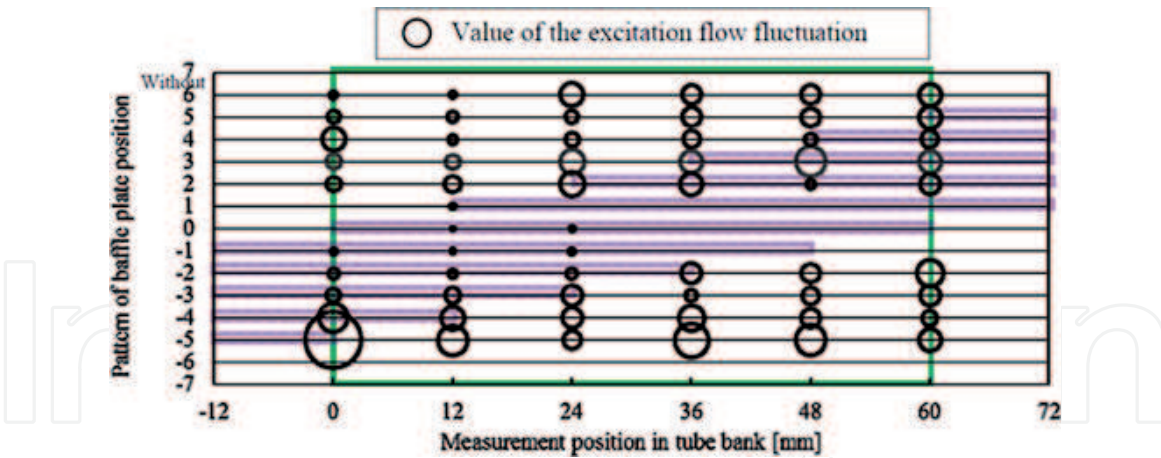
The distribution of the excitation flow fluctuation in the tube bank when the self-sustained tone is generated is examined. Here, it has been non-dimensionalized as shown in Eq. (4) because the excitation flow fluctuation is a value depending on the flow velocity.

$$u = U_f / V_g \tag{4}$$

Figure 20 represents the distribution of the excitation flow fluctuation in the tube bank. The vertical axis shows the baffle plate positions. The circle shows the dimensionless excitation flow fluctuation and its radius indicates the value of the excitation flow fluctuation while the horizontal axis shows the measurement

Figure 19.
The fluctuation velocity of flow and the sound pressure level at observation point ③ with the baffle plate (Pattern of baffle plate position is "0") ([26]).

Figure 20.
Fluctuation velocity of flow on tube bank and the measurement position ([12]).

position of the flow fluctuation velocity in the tube bank. As represented in **Figure 20**, the excitation flow fluctuation is not generated in the entire tube bank under the condition where the self-sustained tone is not generated. On the other hand, **Figure 20** represents that it is generated in the entire tube bank under the condition of the self-sustained tone being generated. Therefore, the two parameters particle velocity and the excitation flow fluctuation are controlled by inserting the baffle plate. Ishihara et al. [12] thought that it is the suppression mechanism of the self-sustained tone to decrease the sound power by controlling these two parameters.

## 4. Countermeasure for self-sustained tone using perforated plate

4.1 Setup of experiment

In this section, we describe the experiments performed by Ishihara and Nakaoka [13] and Ishihara [28]. They carried out some experiments to examine the suppression effect of the perforated plates and cavities installed, and confirmed the suppression effect. They defined the aperture ratio ϕ of the perforated plate and investigated how the change in the value of the aperture ratio ϕ of the perforated plate affects the self-sustained tone in the duct. They varied the value of the aperture ratio ϕ from 1 to 32%. The setup of the experiment is shown in **Figure 21**. The duct is made of acrylic plates that have a thickness of 1 cm. The tube bank consists of an array of bronze tubes whose diameter is D = 6 mm. The array geometry is represented in **Figure 3(b)**, where the spacings T/D and L/D are 2.0. In the tube bank, there are 9 rows of tubes in the flow direction and 19 tubes in the width direction, which is perpendicular to the flow, and the length in the flow direction is 102 mm. The sound pressure signal is measured using the microphone set near the duct outlet as shown in **Figure 3(a)**, and converted to frequency domain with FFT analyzer.

The perforated plate is made of iron, and has a length of 400 mm, a height of 250 mm, and a thickness of 2.3 mm. A hole with a diameter of 3 mm was opened in a staggered arrangement on a plate. As shown in **Figure 22(a)**, perforated plates can be mounted from the slit (shown in green), and the duct has two cavities with a depth of L_c = 100, 66 and 33 mm. In this experiment, in order to examine the influence of the aperture ratio of the perforated plate on the self-sustained tone suppressing effect, as shown in **Figure 22(b)**, assuming a hole diameter of 3 mm, Ishihara and Nakaoka [13] made six patterns (1, 2, 4, 8, 16, and 32%) of the perforated plates. Here, the aperture ratio ϕ is the ratio of the area of the holes to the total area of the perforated plate and is defined by Eq. (5).
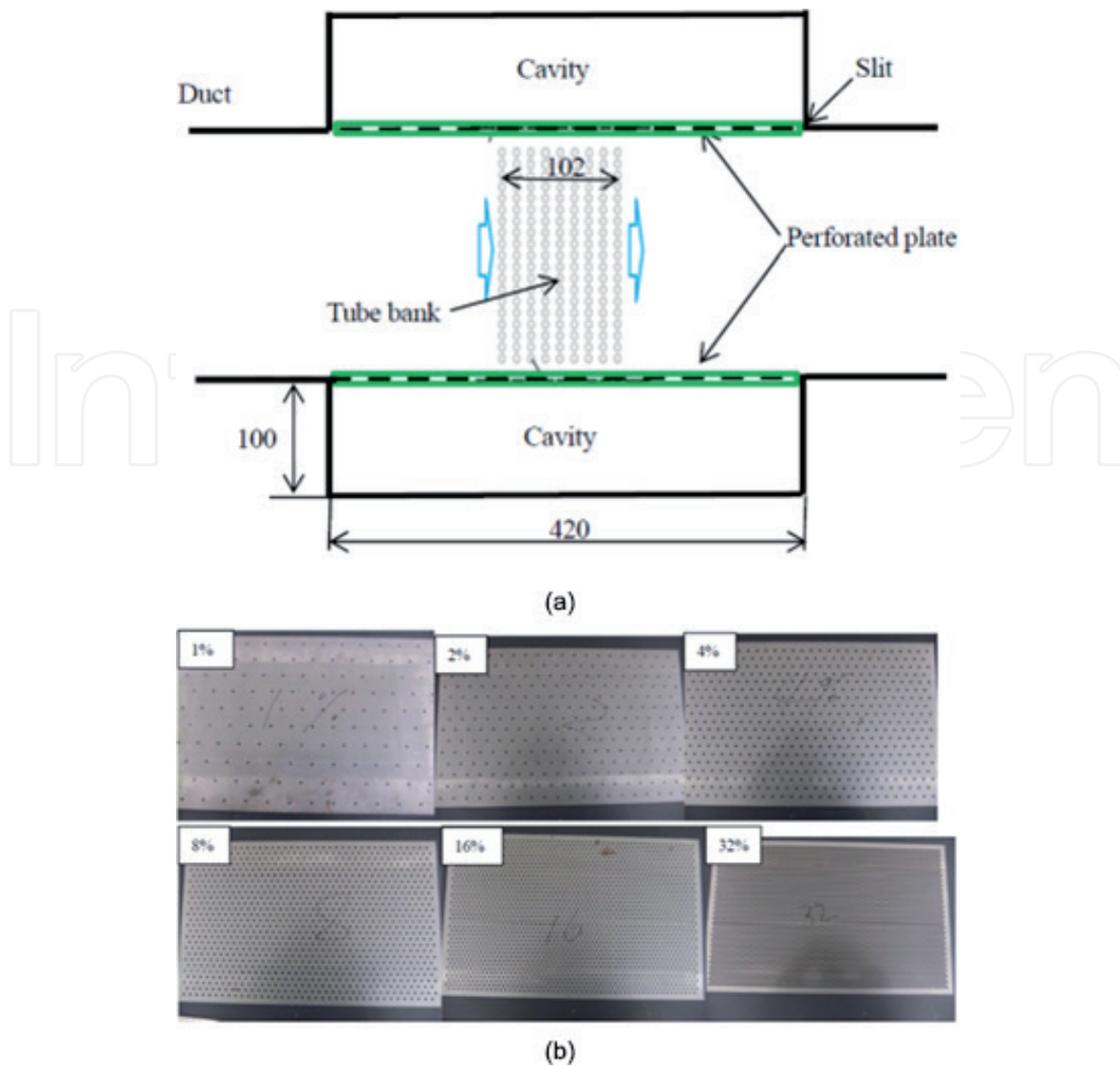
$$\phi = \frac{n_h\left(\frac{\pi d^2}{4}\right)}{S_p} \tag{5}$$

Here, n_h is the number of the hole, Sp = 200 × 420 mm is the total area of the perforated plate, and d is the hole diameter (3 mm). Even at the same aperture ratio, if the hole diameter is different, the influence on self-sustained tone may be different. However, in this study, it is assumed that the hole diameter is constant
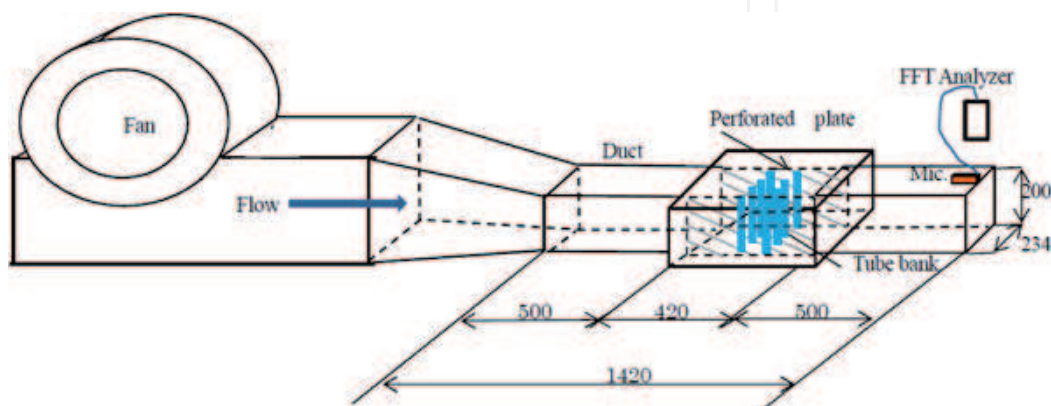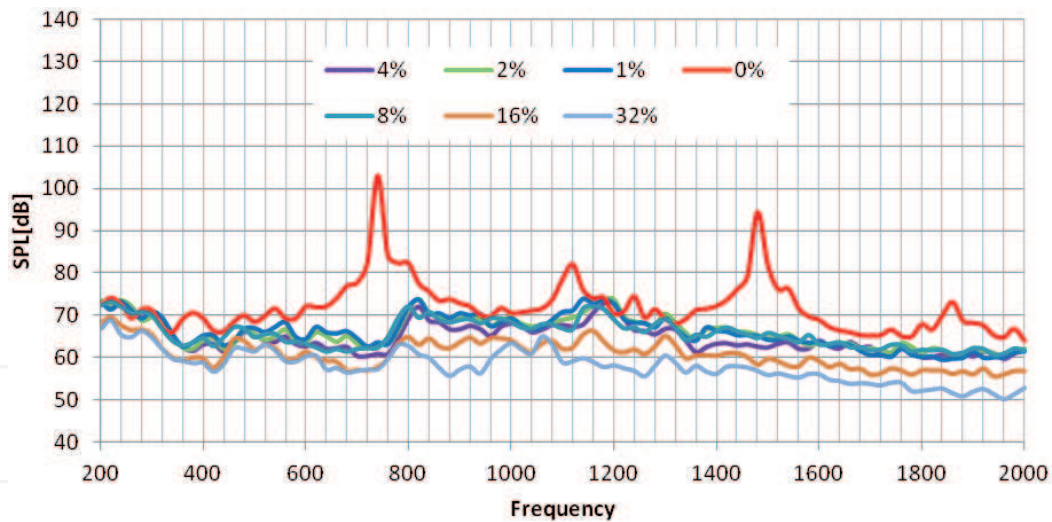

Figure 21.
Setup of experiment [29].

Figure 22.
Tube bank part with perforated plates ([29]). (a) Detail of tube bank part with perforated plates and cavities. (b) Perforated plate.

(3 mm) [13]. Since the case that the aperture ratio is 0% (holeless plate) is defined as the standard of this experiment, ϕ = 0% is also a parameter of the aperture ratio.

4.2 Results of experiments

An effect of the aperture ratio on sound pressure level spectra at the gap velocity V_g = 21.3 m/s is represented in **Figure 23**. The sound pressure decreases more than 30 dB in cases where the perforated plates and cavities are installed ($\phi \geq 0\%$), and the sound pressure level decreases in the high-frequency region as the aperture ratio increases. Hence, the perforated plate is assumed to have a sound-absorbing property at high frequencies. The experimental results of the relation between overall sound pressure level and the gap velocity in cases of aperture ratios ϕ = 1, 2, 4, 8, 16, and 32% are represented in **Figure 24**. Sound following the 5th power law is the ordinary aerodynamic sound, as mentioned in Section 2.3. On the other hand, as shown by the blue circle in **Figure 24**, the noise which does not follow the power law and becomes extremely large is referred to as the self-sustained tone. As shown in **Figure 24**, the self-sustained tone is generated only in the duct with the plate of the aperture ratio ϕ = 0%, which is the normal duct without holes. When the perforated plate with aperture ratios of ϕ = 1–32% is applied on the duct wall surfaces, the overall sound pressure level rises as per the 5th power law, and the self-sustained tone is not generated.
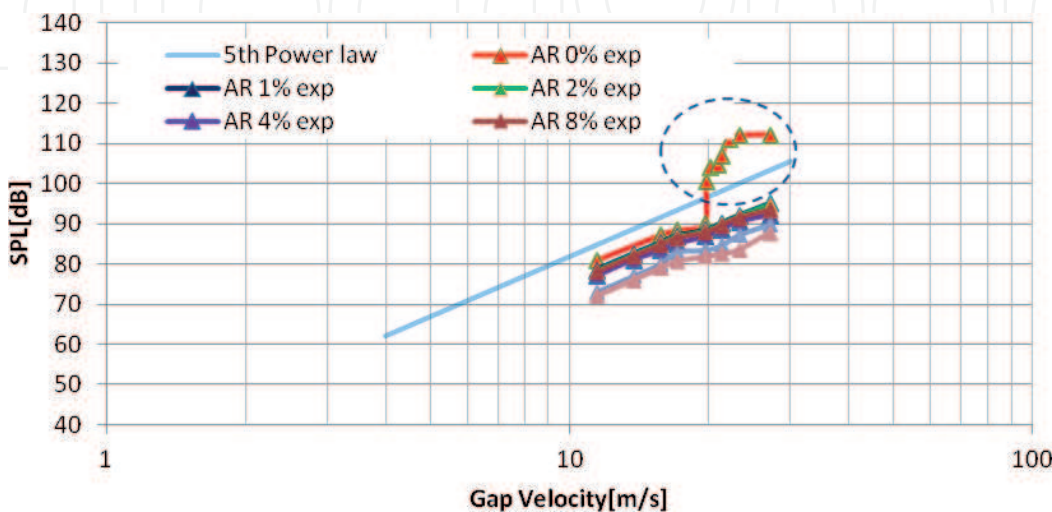
Figure 23.
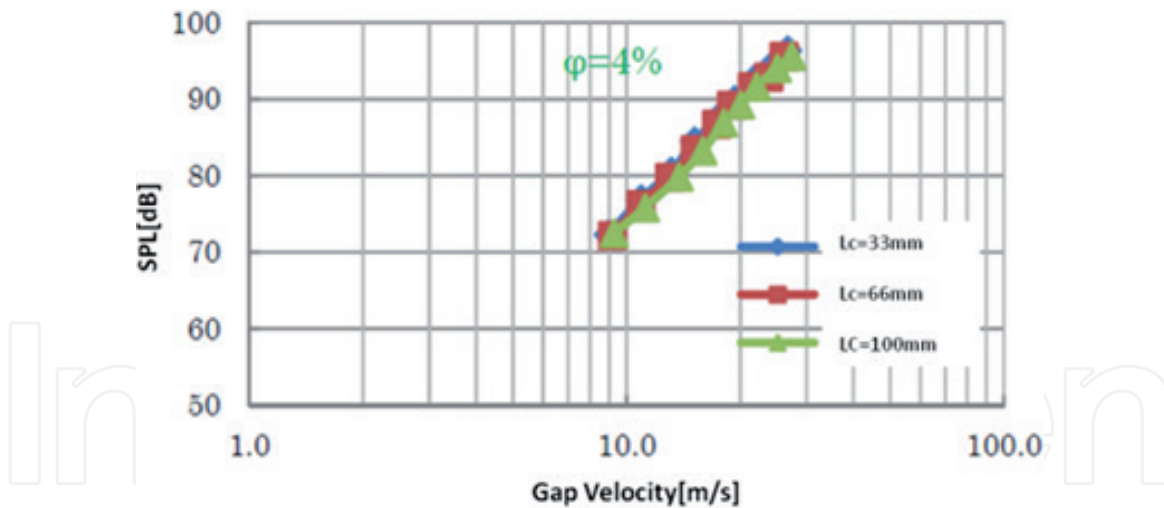*Effect of aperture ratio on sound pressure level spectra at V_g = 21.3 m/s.*

Ishihara [28] studied experimentally the effect of a cavity volume which is used with perforated plates on the SPL. He concluded that the effect of a cavity volume on the SPL is a little. **Figure 25** shows the effect of a cavity volume or depth on the sound pressure level in the case of the aperture ratio ϕ = 4% as the typical example of the aperture ratio. Further, Ishihara [28] clarified experimentally the critical and optimum aperture ratios. The results show that the critical aperture ratio is about 0.25%, and the optimum aperture ratio is concluded to be 4%.

4.3 Unsteady CFD simulations

Mori et al. [29] performed compressible CFD simulations and acoustic simulations, and compared the simulation results with the measurements [13] to numerically verify the effect of the aperture ratio of the perforated plate on the self-sustained tone and acoustic resonance frequencies. The numerical method for unsteady CFD simulations is described in Section 2.4. The CFD model for the normal duct without holes, which corresponds to the duct with the perforated plates of the aperture ratio ϕ = 0%, is shown in **Figure 6**. As an example of the CFD model for the duct with the perforated plates, **Figure 26(a)** represents the CFD model

Figure 24.
Relation between overall sound pressure level and the gap velocity in cases of aperture ratios $\phi(AR)$ = 0, 1, 2, 4, 8, 16, and 32%, and L_c = 100 mm.

17

Figure 25.
Relation between overall sound pressure level and the gap velocity in cases of aperture ratios ϕ = 4% and L_c = 100, 66, and 33 mm [29].

for the duct with the perforated plates of the aperture ratio ϕ = 2%. **Figure 26(b)** shows a part of the CFD model near the perforated plates and cavities in the case of the aperture ratio ϕ = 2%. The CFD domain contains 10,727,088 cells and 6,612,429 nodes for the case of the aperture ratio ϕ = 1%; 12,053,432 cells and 7,308,716 nodes for the case of the aperture ratio ϕ = 2%; and 13,646,420 cells and 8,004,142 nodes for the case of the aperture ratio ϕ = 4%, respectively.

Figure 27 shows instantaneous snapshots of the fluctuation pressure field. Comparing the cases of ϕ = 0% with ϕ = 1%, the fluctuation pressure in the case of ϕ = 0% is much larger than that in the case of ϕ = 1%. In the cases of ϕ = 1%, the pressure fluctuation does not represent the resonance mode in the duct width direction which appears in the case of ϕ = 0% in **Figure 27(a)**.

The effect of the aperture ratio on the frequency spectra of SPL monitored on the wall of the duct near the outflow boundary is represented in **Figure 28(a)**. For comparison, both the simulated and measured data are represented, and the frequency spectra of SPL in the case of ϕ = 0% is also displayed in **Figure 28(a)**. In both simulations and experiments, the self-sustained tone is generated in the case of ϕ = 0%; however, the self-sustained tone is not generated in the cases of ϕ = 1%. The effect of the aperture ratio on the overall sound pressure level is represented in
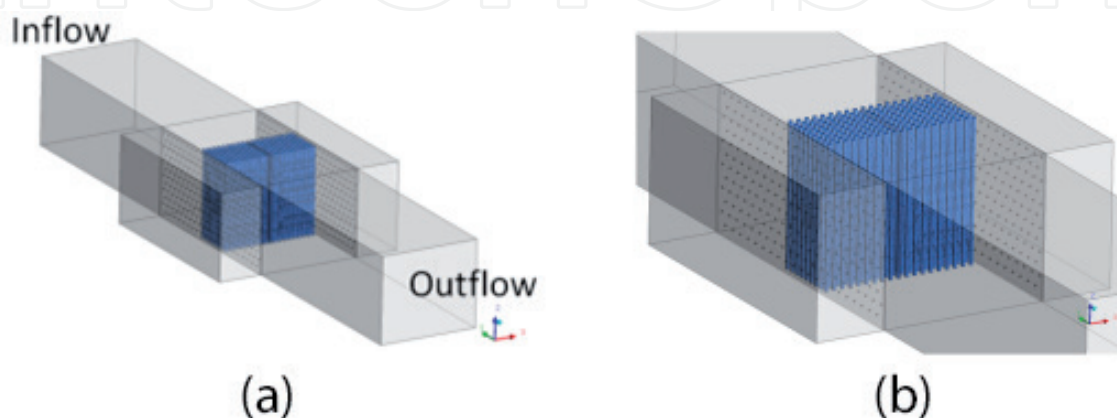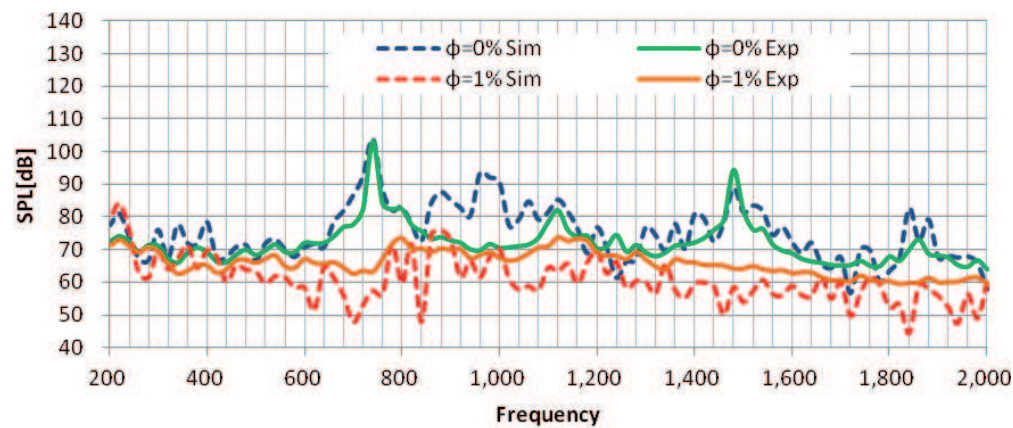

Figure 26.
CFD model for duct with perforated plates and cavities with a depth of L_c=100 mm. (a) Duct with the perforated plates of the aperture ratio ϕ = 2%. (b) Duct near the perforated plates and cavities in the case of the aperture ratio ϕ = 2% [29].
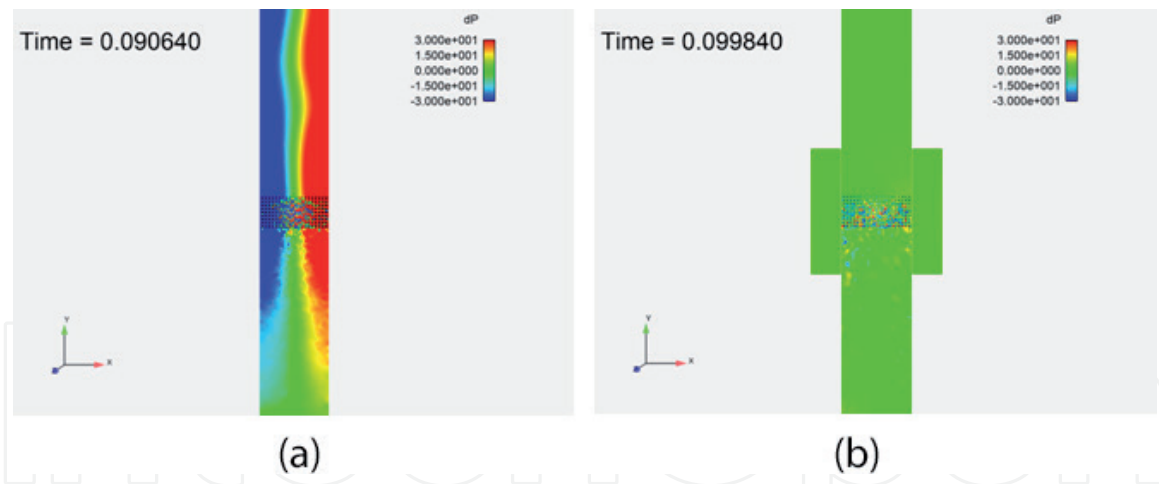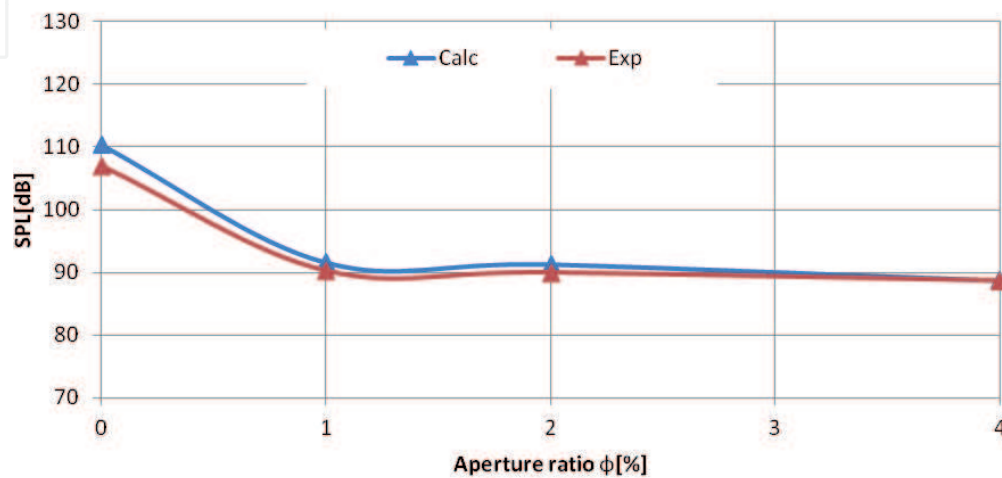
Figure 27.
Fluctuation pressure fields in the cases of aperture ratio at V_g = 21.3 m/s. (a) ϕ =0%. (b) ϕ = 1%.

Figure 28(b). The SPL decreases with an increase of the aperture ratio, and rapidly decreases when the aperture ratio is between 0 and 1%.

Figure 29 shows the SPL on the wall of the duct in frequency domain at the peak frequency, 740 Hz. In the case of ϕ = 0%, the SPL on the wall of the duct clearly represents the acoustic mode in the duct width direction as represented in **Figure 27(a)**. On the other hand, in the cases of ϕ = 1%, **Figure 29(b)** shows that
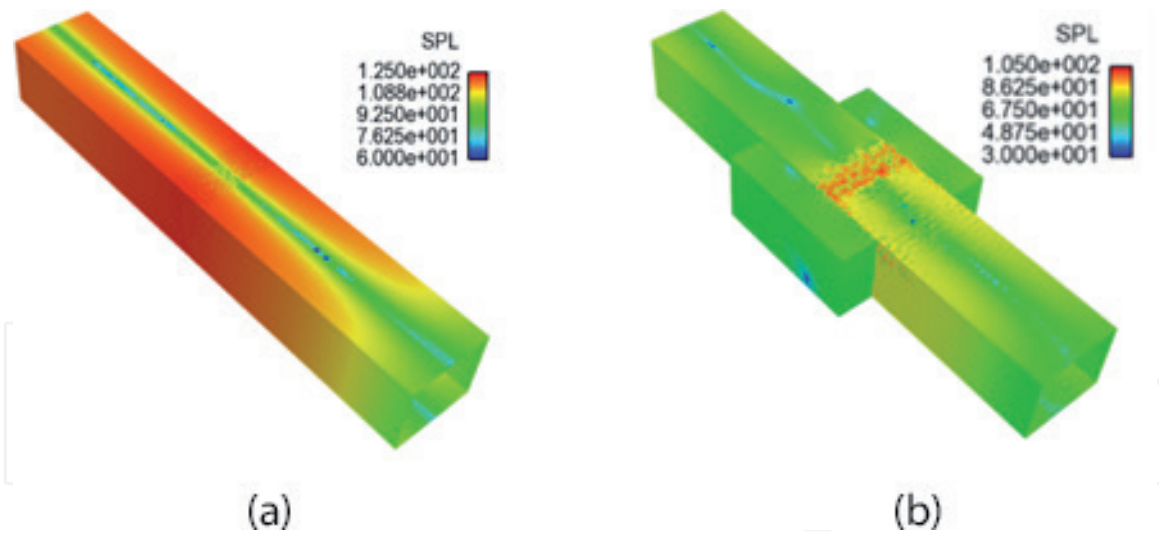

Figure 28.
*Effect of aperture ratio on SPL at V_g = 21.3 m/s. (a) ϕ = 1%. (b) Overall SPL (200–2000 Hz).*

Figure 29.
SPL on the wall of the duct at Vg = 21.3 m/s [29]. (a) ϕ = 0%. (b) ϕ = 1%.

the acoustic mode is not clearly represented and the value of SPL on the duct wall is close to 40 dB smaller than that in the case of ϕ = 0%.

The relation between overall sound pressure level and the gap velocity in the cases of ϕ = 0 and 1% is represented in **Figure 30**. As represented in **Figure 30**, the self-sustained tone is generated in the case of ϕ = 0%, and the sound pressure level does not follow the 5th power law when the gap velocity is high, as mentioned in Section 2.4. However, in the case of ϕ = 1%, the self-sustained tone is not generated, and regardless of the gap velocity, the overall sound pressure level rises along the 5th power law in both simulations and experiments. Therefore, when the perforated plate is installed on the duct wall surfaces, the self-sustained tone is not generated in the CFD simulations, as in the experiments [13].

4.4 Acoustic simulations and suppression mechanism of self-sustained tone by perforated plates

The acoustic characteristics of the duct with the perforated plates and cavities without the flow were calculated by means of BEM (the commercial code, WAON) [30]. Boundary element models for the cases of the aperture ratio ϕ = 0 and ϕ = 2% are shown in **Figure 31(a)** and **(b)**, respectively, and in the case of ϕ = 2%, the duct
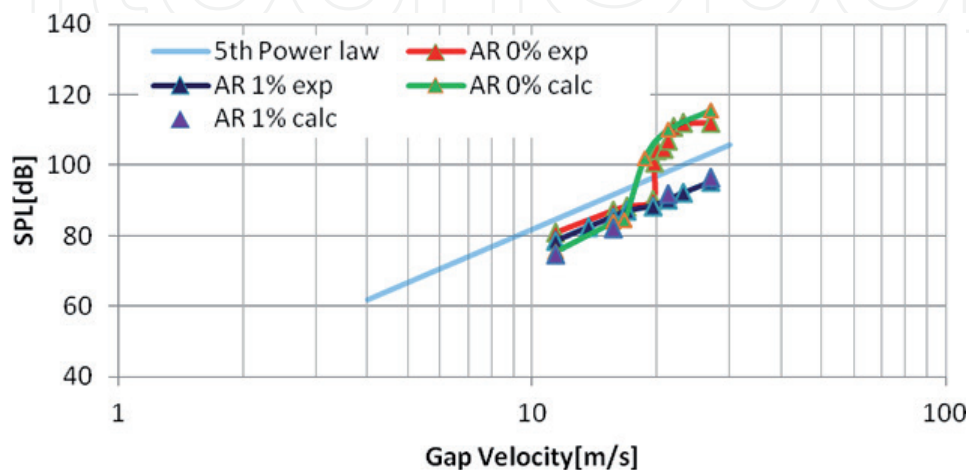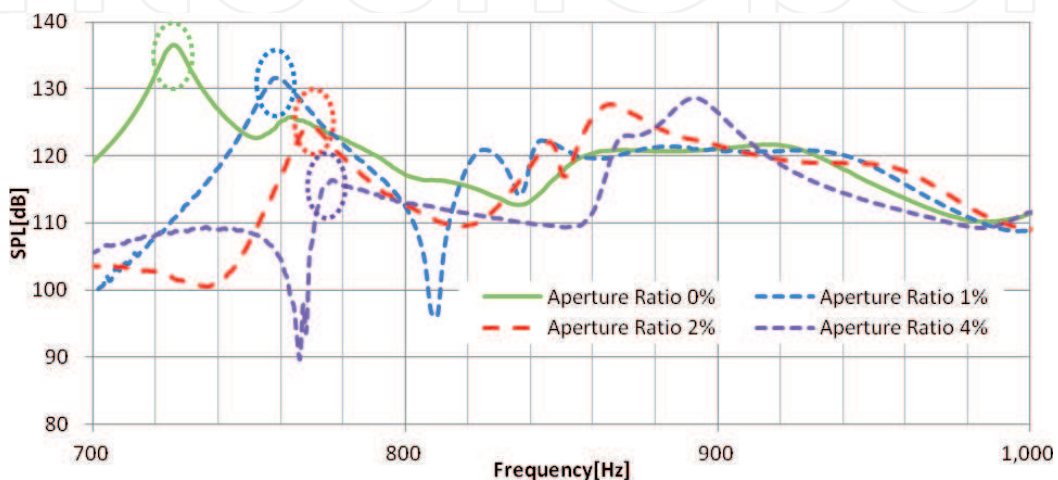

Figure 30.
Relation between overall sound pressure level (200–2000 Hz) and gap velocity in cases of aperture ratios ϕ = 0% and ϕ = 1%.
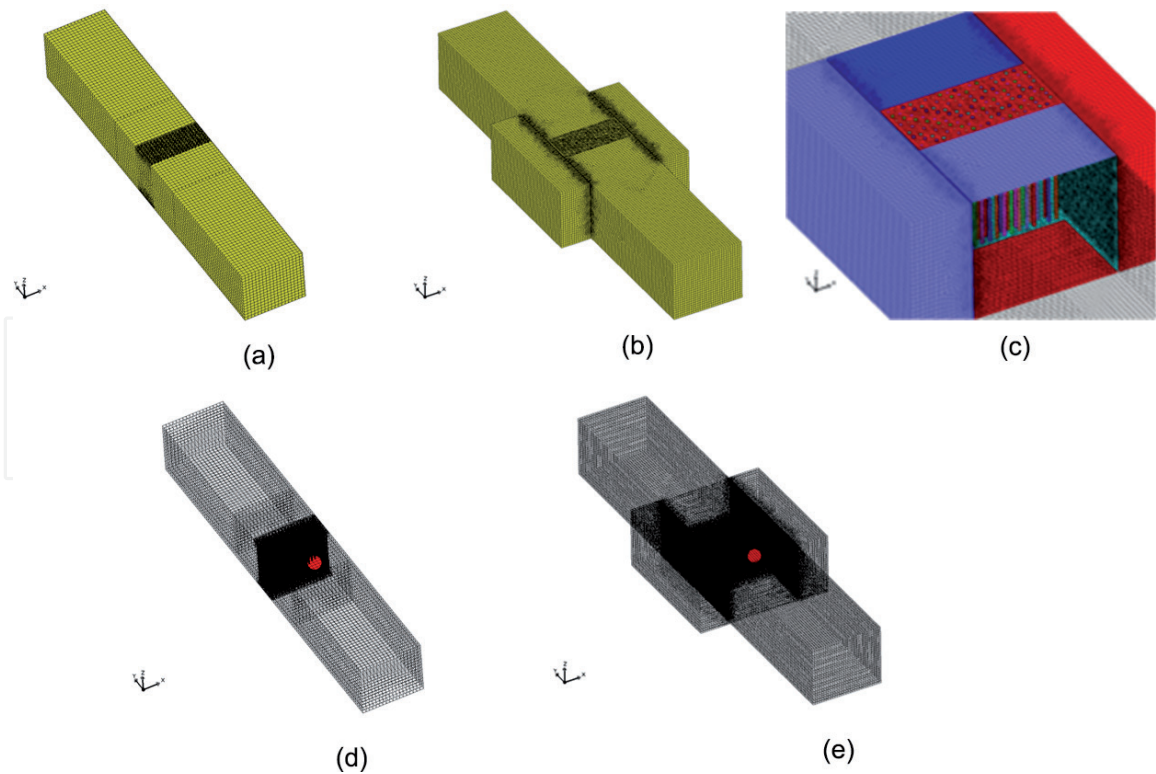
Figure 31.
Boundary element model and position of monopole point source [29]. (a) φ = 0%. (b) φ = 2%. (c) φ = 2%. (d) φ = 0%. (e) φ = 2%.

with the perforated plates and cavities is modeled as shown in **Figure 31(c)**. There are 80,530 boundary elements for the case of the aperture ratio ϕ = 0%; 167,361 boundary elements for the case of the aperture ratio ϕ = 1%; 226,079 boundary elements for the case of the aperture ratio ϕ = 2%; and 307,747 boundary elements for the case of the aperture ratio ϕ = 4%, respectively. The maximum element size is 0.013 m. An impedance boundary condition is imposed at the inflow boundary to consider acoustic waves moving from the inflow boundary to the outside and the value of the impedance is ρc. The outflow boundary is the surface connecting the duct inside and outside. At the outflow boundary, the interface boundary, where the particle velocity and acoustic pressure of the internal and external sound fields of the duct are coupled, is imposed. At other wall boundaries except the holes, weak absorption boundaries, whose absorption coefficient is 0.02, are imposed. The absorption coefficient "0.02"
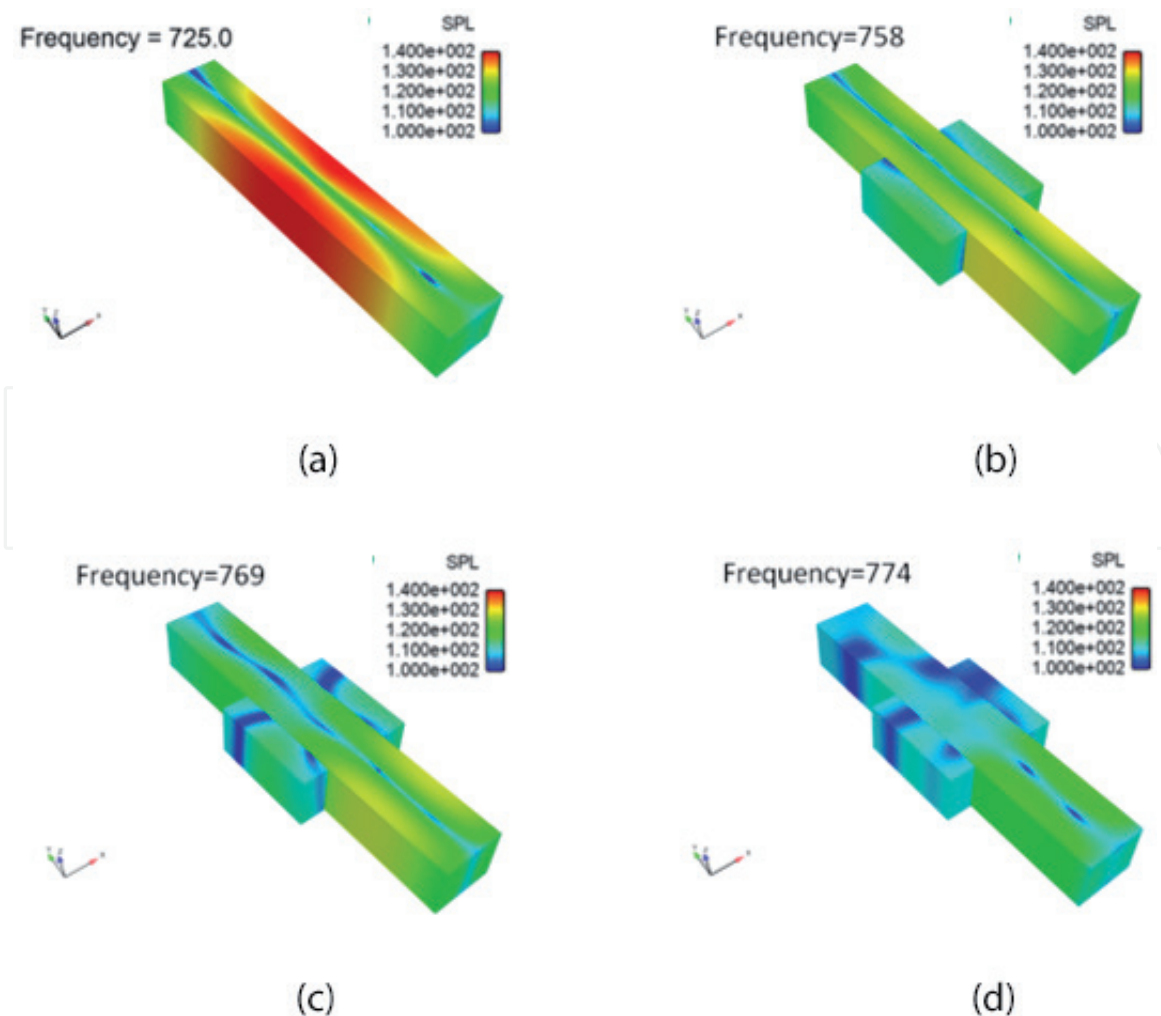

Figure 32.
Acoustic frequency responses.

21

Method, Aperture Ratio	Resonance Frequency
Theory (Aperture Ratio 0 %, without flow)	726.5 Hz
BEM (Aperture Ratio 0 % without flow)	725 Hz
BEM (Aperture Ratio 1 % without flow)	758 Hz
BEM (Aperture Ratio 2 % without flow)	769 Hz
BEM (Aperture Ratio 4 % without flow)	774 Hz

Table 2.
Peak frequency in each case of the aperture ratio [29].

corresponds to that of the general acrylic surface. To clarify the acoustic characteristics of the tube bank duct, the acoustic frequency responses have been calculated using the monopole point sources (without the flow) that are supposed to be vortices generated on the downstream side behind the tube as shown in **Figure 31(d)** and **(e)**. The magnitude of the point sources is 1 Pa at all frequencies. The point source is located at (0.25H, −3.86H, 0) downstream of the tube bank, and H is 200 mm in the height of the tube bank duct. In order to excite the resonance mode in the duct width direction, the sound source was arranged asymmetrically with respect to the YZ plane.

Figure 32 represents the acoustic frequency responses that have been calculated using the monopole point source (without the flow). The monitor point is located

Figure 33.
Acoustic modes at each peak frequency [29]. (a) ϕ = 0%. (b) ϕ = 1%. (c) ϕ = 2%. (d) ϕ = 4%.

at (0.585H, −4.76H, 0) downstream of the tube bank. In the case of ϕ = 0%, the peak frequency surrounded by the green circle is 725 Hz, and close to the resonance frequency in the duct width direction, as mentioned in Section 2.3. On the other hand, in the cases of ϕ = 1, 2, and 4%, peak frequencies surrounded by blue, red, and purple circles are close to the resonance frequency in the duct width direction, and change to higher frequencies than that in the case of ϕ = 0% with an increase of the aperture ratio. **Table 2** represents the peak frequency in each case of the aperture ratio. It has been also confirmed that the resonance frequency increases as the aperture ratio increases in the previous study [31] in which an acoustic resonance frequency has been experimentally and analytically verified by assuming a one-dimensional sound field in a duct partitioned by a perforated plate, and similar results are obtained in this study. **Figure 33** shows the acoustic mode at each peak frequency in the cases of ϕ = 0, 1, 2, and 4%. In the case of ϕ = 0%, the acoustic mode in the width direction strongly appears at 725 Hz. However, in the cases of ϕ = 1, 2, and 4%, the acoustic mode in the duct width direction does not clearly appear, and the value of SPL decreases as the aperture ratio increases. Therefore, it was assumed that the perforated plate has an effect of attenuating sound.

5. Conclusions

1. The sound pressure level rises with an increase of the gap flow velocity by following the 5th power law when the gap velocity is low. However, when the gap velocity is high, the self-sustained tone is generated not by following the 5th power law.

2. Insertion of baffle plates in the tube bank decreases the natural frequency of the duct and increases the onset gap velocity of the self-sustained tone. Hence, the natural frequency of the duct does not seem to be related with the suppression of the self-sustained tone when the baffle plate is installed in the tube bank. The self-sustained tone is the most effectively suppressed by inserting the baffle in the entire tube bank because the baffle plate decreases the particle velocity and vorticity. Furthermore, there is a difference in the onset gap velocity of the self-sustained tone between when the baffle plate is inserted upstream and when it is inserted downstream.

3. The perforated plates installed on the duct walls suppress the self-sustained tone and increase the resonance frequency in the duct width direction. Consequently, if the perforated plates are installed on the duct walls, the self-sustained tone is assumed to be suppressed by an increase of the resonant frequency in the duct width direction and sound-absorbing effect of the perforated plates.

Author details

Masaaki Mori[1*] and Kunihiko Ishihara[2*]

1 Cybernet Systems CO., LTD, Tokyo, Japan

2 Department of Health and Welfare, Tokushima Bunri University, Japan

*Address all correspondence to: m-mori@cybernet.co.jp

IntechOpen

References

[1] Baird RC. Pulsation-induced vibration in utility steam generation unit. Combustion. 1954;**25**:38-44

[2] Owen PR. Buffeting excitation of boiler tube vibration. Journal of Mechanical Engineering Science. 1965;**7**(4):431-439

[3] Chen YN. Flow-induced vibration and noise in tube-bank heat exchangers due to von karman streets. Journal of Engineering for Industry. 1968;**90**(1):134-146

[4] Fnunakawa M, Umakoshi R. The acoustic resonance in a tube bank. Bulletin of JSME. 1970;**13**(57):348-355

[5] Fitzpatric JA. The prediction of flow-induced noise in heat exchanger tube arrays. Journal of Sound and Vibration. 1985;**99**(3):425-435

[6] Blevins RD, Bresser MM. Acoustic resonance in heat exchanger tube bundles-part 1: Physical nature of the phenomena. Journal of Pressure Vessel Technology. 1987;**109**(3):275-281

[7] Weaver DS. Vortex shedding and acoustic resonance in heat exchanger tube arrays. Technology for the 90's. ASME. 1993:776-810

[8] Hamakawa H, Matsue H, Nishida E, Fukano T. Acoustic resonance and vortex shedding from tube banks of boiler plant. Journal of Fluid Science and Technology. 2008;**3**(6):805-813

[9] Hanson R, Mohany A, Ziada S. Effect of acoustic resonance on the dynamic lift of tube arrays. Journal of Fluids and Structures. 2009;**25**(3):80-94

[10] Ziada S, Oengören A. Vortex shedding in an in-line tube bundle with large tube spacings. Journal of Fluids and Structures. 1993;**7**(6):661-687

[11] Hamakawa H, Matsue H, Nishida E, Fukano T. Effect of arrangement of tube banks on acoustic resonance. Open Journal of Fluid Dynamics. 2012;**2**(4A):311-317

[12] Ishihara K, Tamehira T, Tsujii M, Ichimiya M. Study on a countermeasure of self-sustained tone by a baffle plate in boiler tube banks. Journal of Basic and Applied Physics. 2013;**2**(3):148-154

[13] Ishihara K, Nakaoka M. Study on a countermeasure using walls made of perforated plate for high level sound. In: Proceedings of ASME 2015 Pressure Vessels and Piping Conference Volume 4: Fluid-Structure Interaction

[14] Eisinger FL, Sullivan RE. Suppression of acoustic waves in steam generator and heat exchanger tube banks. Journal of Pressure Vessel Technology. 2003;**125**(2):221-227

[15] Feenstra PA, Weaver DS, Eisinger FL. Acoustic resonance in a staggered tube array: Tube response and the effect of baffles. Journal of Fluids and Structures. 2005;**21**(1):89-101

[16] Hamakawa H, Miyagi H, Nishida E, Fukano T. Effect of small cavities in in-line tube banks on vortex shedding. Transactions of the Japan Society of Mechanical Engineers, Part B. 2010;**76**(764):580-587

[17] Ishihara K, Takahashi T. Reduction of large noise generated in boiler and heat exchanger by flexible walls. Transactions of the Japan Society of Mechanical Engineers. 2013;**79**(802):1837

[18] Ingard U. On the theory and design of acoustic resonators. The Journal of the Acoustical Society of America. 1953;**25**:1037-1045

[19] Melling TH. The acoustic impedance of perforates at medium and high sound

pressure levels. Journal of Sound and Vibration. 1973;**29**(1):1-65

[20] Lawn C. The acoustic impedance of perforated plates under various flow conditions relating to combustion chamber liners. Applied Acoustics. 2016;**106**:144-154

[21] Hanson R, Mohany A, Ziada S. Flow-excited acoustic resonance of two side-by-side cylinders in cross-flow. Journal of Fluids and Structures. 2009;**25**:80-94

[22] Mohany A, Arthurs D, Boldu M, Hassan M, Ziada S. Numerical and experimental investigation of flow-acoustic resonance of side-by-side cylinders in a duct. Journal of Fluids and Structures. 2014;**48**:316-331

[23] Shahab K, Zaffar MK, Muhammad AM, Zafarullah K, Muhammad AJ, Mahmood AK, et al. Cross-Flow-Induced-Vibrations in Heat Exchanger Tube Bundles: A Review, Nuclear Power Plants. Europe: Intech; 2012. 4

[24] Mori M, Masumto T, Ishihara K. Numerical simulation of high level sound generated in boiler tube bank duct. International Journal of Engineering and Applied Sciences. 2018;**5**(1):19-24

[25] Mankbadi R, Lo S-C, Lyrintzis A, Golubev V, Dewan Y, Kurbatskii K. Hybrid LES-RANS simulations of a jet impinging on a flat plate. International Journal of Aeroacoustics. 2016;**15**(4-5):535-553

[26] Ishihara K, Tamehira T, Tsujii M, Ichimiya M. Study on countermeasure mechanism by baffle plate for self-sustained tone generated in boiler tube banks. Transactions of the Japan Society of Mechanical Engineers. 2012;**78**(787):749

[27] Howe MS. The dissipation of sound at an edge. Journal of Sound and Vibration. 1980;**70**(3):407-411

[28] Ishihara K. Study on a countermeasure for high level sound generated from boiler tube bank duct using walls made of perforated plate (Grasp critical aperture ratio and influence of cavity volume on suppression effect). Transactions of the Japan Society of Mechanical Engineers. 2017;**83**(848):456

[29] Mori M, Masumto T, Ishihara K. Numerical verification on a countermeasure for high level sound generated from boiler tube bank duct using walls made of perforated plate and cavity. International Journal of Science and Engineering. 2018;**7**(80):117-130

[30] Mori M, Masumto T, Ishihara K. Study on acoustic and flow induced noise characteristics of t-shaped pipe with square cross-section. Advances in Applied Acoustics. 2016;**5**:10-17

[31] Ishihara K, Kudo S, Masumoto T, Mori M. Study on acoustic natural frequency and its mode of one dimensional sound field partitioned by perforated plate. Transactions of the Japan Society of Mechanical Engineers. 2018;**84**(857):365